www.nature.com/cr
www.cell-research.com

LETTER TO THE EDITOR

Creation of artificial karyotypes in mice reveals robustness of genome organization

Cell Research (2022) 32:1026–1029; https://doi.org/10.1038/s41422-022-00722-x

Dear Editor,

Robertsonian (Rb) fusions contribute to the diversity in species karyotypes. However, how it occurs and propels evolution is still unknown, mainly due to the lack of a simple and efficient method for genetically manipulating chromosomes in animals. While the typical mouse karyotype (2n = 40) is completely telocentric except chromosome Y (ChrY), the western European subspecies *M. m. domesticus* contains diverse chromosomal races, with a diploid number varying between 38 and 22 due to carrying one or multiple pairs of metacentric chromosomes, which results from the Rb fusions between two telocentric chromosomes.[1] Recapitulation of this process in the laboratory may help to shed light on the function of Rb fusions in evolution. The detailed mechanisms underlying Rb fusion in *M. m. domesticus* requires further investigations,[2] but previous studies have shown that Rb fusion-induced metacentric chromosomes have a neo-centromeric region of minor satellite (MinSat) sandwiched between two large blocks of major satellite (MajSat) DNA.[3] These observations imply that Rb fusion breakpoints are localized within the MinSat sequences of the centromeric region. Given that CRISPR-Cas9-mediated chromosome engineering has successfully fused 16 yeast chromosomes through head-to-tail strategies to produce yeast strains with 1 or 2 chromosomes,[4,5] we hypothesize that CRISPR-Cas9-mediated chromosome engineering through targeting MinSat sequences could be an ideal strategy for creating mouse strains with reduced chromosome numbers in the laboratory.

Mouse MinSat monomers are highly homogeneous among different chromosomes, consist of tandem repeats of a 120-bp monomer unit, and locate exclusively to the centromere of all chromosomes except ChrY.[6] Here, we designed 5 sgRNAs targeting different regions in the MinSat of centromere (termed CENsg1–CENsg5, Fig. 1a). We first tested the feasibility of generating CRISPR-Cas9-mediated chromosome fusions in the mouse embryos by directly injecting Cas9 mRNA and each of the 5 sgRNAs into zygotes. However, all 5 sgRNAs, even at low concentrations, impaired blastomere division and caused developmental arrest at early embryonic stages, probably due to the dramatically increased DNA damage response (DDR) in the pronucleus of injected zygotes (Supplementary information, Fig. S1a–f).

Mouse androgenetic haploid embryonic stem cells (AG-haESCs, also termed sperm-like stem cells) that carry only sperm genome are feasible for CRISPR-Cas9-mediated genetic manipulations, leading to the production of semi-cloned mice (SC mice) with corresponding genetic traits in one step through intracytoplasmic injection into oocytes (ICAHCI).[7,8] After transfection of CRISPR-Cas9 and CENsg into haploid cells (a cell line termed O48 that can efficiently support SC mouse generation), we observed much weaker DNA damage signals compared to those in injected zygotes (Supplementary information, Fig. S2a, b). Karyotyping analysis showed that while > 97% cells sustained a normal karyotype, the rest of cells carried chromosomal fusions, in which more than half were non-homologous Rb fusions that may result in metacentric chromosomes (Supplementary information, Fig. S2c). Moreover, CENsg1 displayed the highest efficiency (Fig. 1b), which was selected for our subsequent targeting experiments.

A total of 1128 cell clones from 12 transfection experiments were employed for karyotyping analysis (Supplementary information, Fig. S2d). In summary, we acquired 10 stable haploid ESC lines carrying 19 chromosomes, which consist of one metacentric chromosome and 18 telocentric chromosomes (termed ROB-O48 cells) (Fig. 1c; Supplementary information, Figs. S2e, S3a). Rb fusions did not affect the maintenance of haploidy in ROB-O48 cells, and the metacentric chromosomes could stably exist in ROB-O48 cells during long-term in vitro culture (up to 50 passages) (Supplementary information, Fig. S3b, c). Moreover, whole-genome sequencing (WGS) of 4 ROB-O48 cell lines and wild-type (WT) O48 cells indicated normal karyotype features, except RXn2 (Rb fusion between ChrX and Chr2) cells, which carried segmental duplications in Chr14 (Supplementary information, Fig. S3d). Together, these results indicate that CRISPR-Cas9-mediated cleavage at MinSat of centromere can successfully induce head-to-head fusion between two telocentric chromosomes in sperm-like stem cells.

DNA FISH analysis showed that while Chr2 and Chr6 were located in a separate space within the nucleus of WT O48 cells, the distance between two fused chromosomes was diminished in R2n6 cells (Fig. 1d; Supplementary information, Fig. S4a). Similar results were observed in other tested ROB-O48 cells (Supplementary information, Fig. S4b, c). Meanwhile, we observed that the neo-centromere consisted of a MinSat flanked by MajSat at both sides but no telomere DNA between two fused chromosomes in all ROB-O48 cells (Fig. 1e), consistent with previous observations in the natural metacentric races.[2] Interestingly, two MinSat-enriched regions were observed in all metacentric chromosomes containing Chr2 (dicentric chromosomes) (Fig. 1f; Supplementary information, Fig. S5a, b). As expected, we found that Chr2 indeed has two centromeres in the proximal region (*p*-arm) in O48 cells, including one small centromere (termed sCEN, closely adjacent to the chromosome arm and enriched with only mutant MinSat[9]) and one big centromere (termed bCEN, surrounded by the pericentromeric region and enriched with both WT and mutant MinSat) (Supplementary information, Fig. S5c–e). The activity analysis of two centromeres indicated that while sCEN was inactivated as it was only bound by centromere protein B (CENP-B), bCEN was active as revealed by colocalization with both CENP-B and CENP-A that is only seen at active centromeres (Fig. 1g; Supplementary information, Fig. S5f, g).[10] These results indicate that the sCEN has been inactivated during evolution, consistent with previous observations that two active

Received: 11 August 2022 Accepted: 30 August 2022
Published online: 20 September 2022

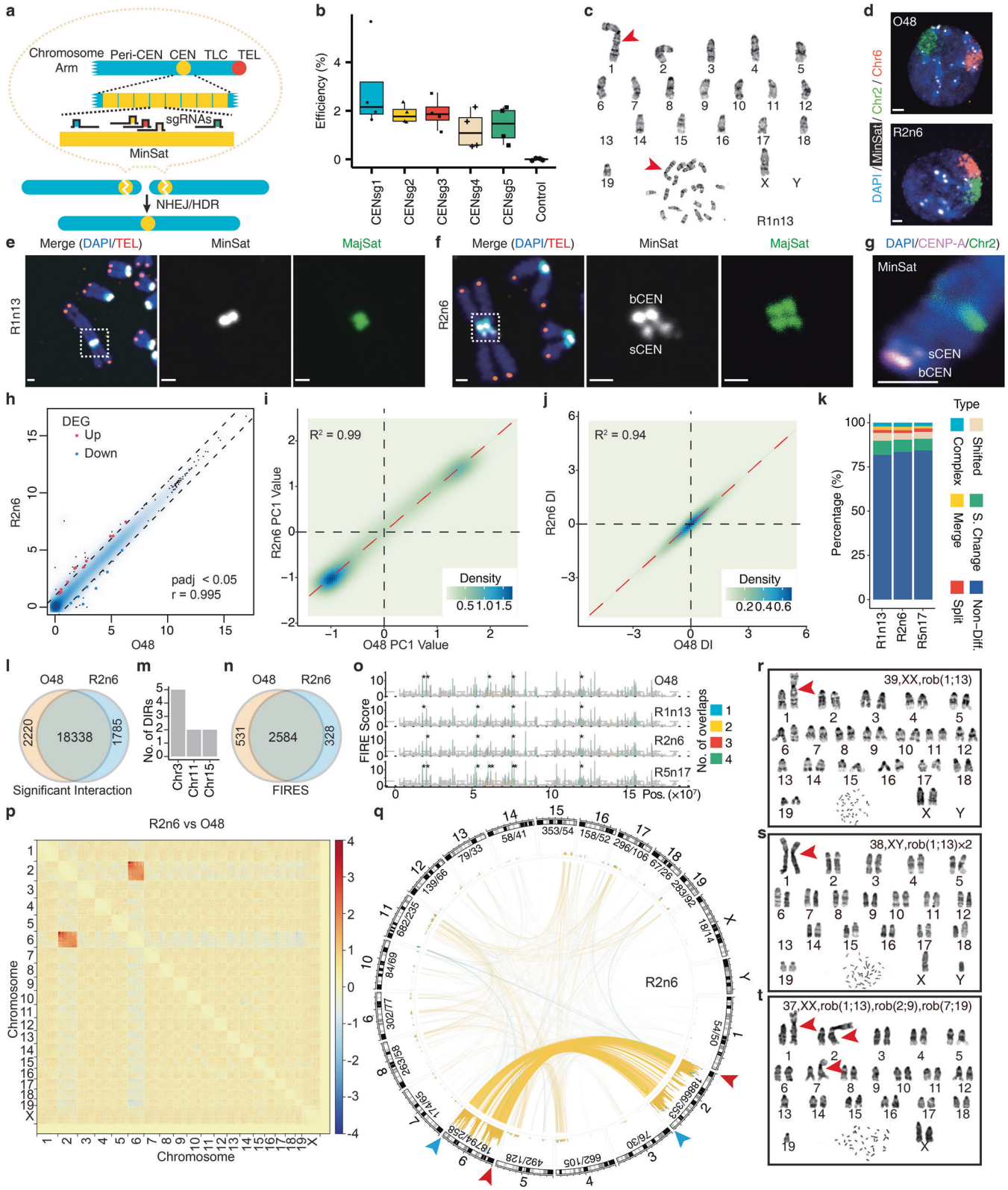

centromeres in dicentric chromosomes may induce mitotic instability.[11]

ROB-O48 cells showed colony morphology and expressed the typical ESC markers similar to AG-haESCs (Supplementary information, Fig. S6a). Teratoma analysis showed that tissues of three germ layers could be formed upon differentiation, indicating that the pluripotency is well preserved in ROB-O48 cells (Supplementary information, Fig. S6b). Strikingly, RNA-sequencing (RNA-seq) results revealed a high correlation between ROB-O48 cells and O48 cells based on pluripotency-related genes or all expressed genes (r = 0.99) (Fig. 1h). Only a few differentially expressed genes (DEGs) were identified in ROB-O48 cells with one

Fig. 1 Creation of mouse models with artificial karyotypes via sperm-like stem cells. a Up, diagram of the proximal region of mouse chromosome, including telomere (TEL, red dot), telocentric (TLC) tandem repeats, centromere (CEN, yellow dot), pericentromeric region (Peri-CEN), and gene-rich chromosome arm. Five sgRNAs were designed for targeting the MinSat repeats of CEN. Bottom, diagram of induced Rb fusion between two chromosomes after cleavage of centromeres. **b** Efficiency of Rb fusions induced by 5 sgRNA (CENsg1–CENsg5). Colored boxes are corresponding to sgRNAs shown in **a**. Four independent experiments (each with 500 karyotypes) were performed for each CENsg. **c** Representative karyotype image showing an established haploid cell line (R1n13) with one metacentric chromosome fused between Chr1 and Chr13. **d** Representative images of Chr2 and Chr6 distributions in O48 ($n = 34$) and R2n6 ($n = 37$) cells analyzed by immunostaining with chromosome-specific probes. Green, Chr2; orange, Chr6; blue, chromosomes; white, MinSat. **e** DNA FISH of R1n13 cells showing that the neo-centromeric region consists of one MinSat-enriched centromere (gray) surrounded by MajSat-enriched pericentromere (green). No telomere sequences (orange) were detected in the neo-centromere. Box with the white dotted line in the left image is magnified in the right images. 25 images were analyzed. Scale bars, 1 μm. **f** DNA FISH of R2n6 cells showing that neo-centromeric region contains two separated MinSat-enriched centromeres (gray). The small one (sCEN) is adjacent to chromosome arm and the big one (bCEN) is in the middle of the neo-centromeric region and surrounded by MajSat-enriched pericentromere (green). Box with the white dotted line in the left image is magnified in the right images. 42 images were analyzed. Scale bars, 1 μm. **g** Cell line termed CENP-A-HAtag generated by insertion of HA (human influenza hemagglutinin) tag sequence into 3′-terminus of CENP-A sequence was used to analyze the distribution of CENP-A on Chr2 with HA antibody (red) followed by DNA FISH with Chr2-specific probe (green) and MinSat probe (gray). 12 images were analyzed. Blue, DNA (DAPI). Scale bar, 4 μm. **h** Correlation of genome-wide expression patterns between O48 and R2n6 cells. Red and blue dots mark upregulated and downregulated genes, respectively. Pearson correlation of all expressed genes is 0.995. **i** 2D density plot of all O48 and R2n6 PC1 values at 100-kb resolution. Red dash line represents liner regression (Coefficient of determination, $R^2 = 0.99$) of all data points. Pearson correlation of two samples is 0.99 with $P < 2.2E{-}16$. There are no compartment switches between O48 and R2n6 cells. **j** 2D density plot of all O48 and R2n6 directional index (DI) values at 40-kb resolution. Red dash line represents liner regression ($R^2 = 0.94$) of all data points. Pearson correlation of two samples is 0.97 with $P < 2.2E{-}16$. **k** Distribution of the TAD boundary change types between O48 and ROB-O48 cells detected by TADCompare. Non-diff, non-differential type; S. Change, strength change. **l** Overlap of identified significant intra-chromosomal interactions between O48 and R2n6 cells. **m** Numbers of DIRs identified by multiHiCcompare. Resolution, 500 kb. **n** Overlap of identified FIREs between O48 and R2n6 cell lines. **o** FIRE distribution on Chr2 in all samples. FIREs are colored by the number of its presence in all samples. For example, if the FIRE was called in all 4 samples, it was colored green. Stars indicate super-FIREs. **p** Compared matrix between O48 and R2n6 cells showing elevated interactions between fused chromosomes. Resolution, 500 kb. **q** Distribution of changes in significant inter-chromosomal interactions called by FIT-HI-C. Yellow links, interactions gained in ROB-O48 cells; cyan, interactions lost in ROB-O48 cells; numbers and barplots under each chromosome indicate gained/lost inter-chromosomal interactions. Red and blue arrowheads indicate CEN and TEL, respectively. **r** Representative karyotype image of a founder SC mouse (F0 ROB het ♀) derived from R1n13 cells. **s** Representative karyotype image of a male mouse with one pair of metacentric chromosomes derived from R1n13 cells. **t** Representative karyotype image of a founder SC mouse with multiple heterozygous Rb chromosomes from R1n13.R2n9.R7n19 with three metacentric chromosomes. Red arrowheads in **c**, **r**–**t** show metacentric chromosomes.

Rb fusion compared to O48 cells (Supplementary information, Fig. S6c). Interestingly, DEGs were located at both fused chromosomes and unfused chromosomes (Supplementary information, Fig. S6d), suggesting that Rb fusions may introduce mild perturbations in both fused and unfused chromosomes. Together, single chromosome fusion events have a limited effect on the transcriptome and differentiation potential in all tested ROB-O48 cells.

Given that the 3D organization of chromosomes is important for various functions including transcription and evolution, we asked whether Rb fusion-induced large-scale structural reorganizations may alter the chromatin 3D structure by performing in situ high-throughput 3 C (in situ Hi-C)[12] on ROB-O48 cells (R1n13, R2n6, and R5n17.1) and O48 cells with three biological replicates for each cell line (Supplementary information, Fig. S7a, b). First, we compared A/B compartment distribution between ROB-O48 cells and O48 cells, and the results indicated a surprisingly high similarity in first principal component (PC1) values, and no compartment rearrangement was identified in ROB-O48 cells (Fig. 1i; Supplementary information, Fig. S8a–c). Second, > 90% of topologically associating domain (TAD) boundaries in O48 cells could be repeated in ROB-O48 cells and TAD boundary scores in ROB-O48 and O48 cells were highly correlated (Fig. 1j; Supplementary information, Figs. S8c, S9a–d). Moreover, TAD comparison analysis indicated that the majority of the TADs were non-differential type (> 80%) and "noisy" type boundary changes (Strength Change and Shifted types, 10%) (Fig. 1k). Third, ~87% of significant intra-chromosomal interactions could be detected in both O48 and ROB-O48 cells (Fig. 1l; Supplementary information, Fig. S10a–d). We further called differential interaction regions (DIRs) in ROB-O48 compared to O48 cells and found only ~10 significant DIRs, which were distributed evenly along both fused and non-fused chromosomes (Fig. 1m; Supplementary information, Fig. S10e). Finally, the correlation of frequently interacting region (FIRE) scores between O48 and ROB-O48 cell lines was positioned at 0.90–0.99 and most of the detected FIREs could be observed in all samples (Fig. 1n, o; Supplementary information, Fig. S11a–e). Together, Rb fusions only lead to slight fluctuation in genome-wide intra-chromosomal interactions.

Consistent with the observation that Rb fusions directly reduced the physical distance between two fused chromosomes (Fig. 1d; Supplementary information, Fig. S4), we also observed intensified contacts between two fused chromosomes, especially around the newly fused centromere sites (Fig. 1p; Supplementary information, Fig. S12a–c). Next, we called significant inter-chromosomal interactions and found that the major differences between O48 and ROB-O48 cells were at two fused chromosomes, especially near the centromere regions (Fig. 1q; Supplementary information, Fig. S12d). Interestingly, although Chr11 was not involved in Rb fusions, it exhibited more changeable interaction with other chromosomes in all tested ROB-O48 samples (Supplementary information, Fig. S13a). Moreover, we observed an extensive change of interaction at the tail region of Chr2, Chr4, Chr5, and Chr11 (Fig. 1q; Supplementary information, Figs. S12d, S13b). Coincidently, these regions are marked as the active hub that is organized around nuclear speckles.[13] Together, these data indicate that Rb fusions induce elevated inter-chromosomal interactions between fused chromosomes or active hubs, and the genome-wide inter-chromosomal interactions can be readjusted correspondingly.

Having demonstrated that Rb fusions have a limited impact on transcriptome and 3D genome organizations of ROB-O48 cells, we then explored the possibility to generate mouse models by injecting these cells into oocytes. Notably, the results showed that all ROB-O48 cells bearing 19 chromosomes gave rise to live SC animals with one heterozygous metacentric chromosome (Fig. 1r; Supplementary information, Fig. S14a, b). The SC pups from the majority of ROB-O48 cell lines could grow, except that RXn2-originated SC pups died several days after birth, probably due to

fragment duplications in Chr14 (Supplementary information, Table S1). All SC mice were female[7] and delivered the metacentric chromosome to the next generation, and female and male F1 mice carrying one heterozygous metacentric chromosome were obtained (Supplementary information, Fig. S14c). Both heterozygous male and female mice with one Rb chromosome were fertile, leading to four homozygous mouse strains to date with one pair of metacentric chromosomes derived from cell lines of R1n13, R2n6, R2n11, and R5n17.1, respectively (Fig. 1s; Supplementary information, Fig. S14d–k).

Finally, we tested the feasibility of derivation of ROB-O48 cells or mice with multiple fused chromosomes by performing additional CRISPR-Cas9-based Rb fusions in R1n13 cells. A cell line with two metacentric chromosomes was generated (termed R1n13.R2n9), followed by generating three ROB-O48 cells with three fused chromosomes (termed R1n13.R2n9.R7n19, R1n13.R2n9.R7n10, and R1n13.R2n9.R4n14, respectively) (Supplementary information, Fig. S15a). Interestingly, transcriptome analysis showed an increased tendency of DEGs with the accumulation of chromosome fusion events (Supplementary information, Fig. S15b). DEGs were located at both fused and unfused chromosomes (Supplementary information, Fig. S15c). Importantly, these cells could give rise to healthy SC pups with heterozygous metacentric chromosomes, which could also transmit the fused chromosomes to the next generation (Fig. 1t; Supplementary information, Fig. S15d, e and Table S1). Together, these results confirm that single or multiple Rb fusions can be tolerated by the organism and stably transmitted to offspring.

In summary, we have successfully generated mouse models with metacentric chromosomes through CRISPR-Cas9-induced cleavage of MinSat repeats in sperm-like stem cells, providing the direct evidence that the occurrence of breakpoints in minor satellites underlies the natural derivation of metacentric races. Interestingly, zygote injection of CRISPR-Cas9 targeting MinSat cannot produce mice with Rb fusions due to remarkable DDR-induced embryonic developmental arrest. These results suggest that the preexistence of Rb fusions in gametes may account for the naturally occurring mouse strains with reduced chromosome numbers. Our study likely recapitulates the natural derivation of metacentric races formed within 10^2–10^5 years in mice.[14] Therefore, sperm-like stem cell-mediated semi-cloning technology provides an experimental platform for investigating the function of chromosome structures in karyotype evolution.

Our chromosome engineering strategy, in combination with Hi-C technology, enables modeling the chromosomal movements in the nucleus induced by chromosome structure changes, thus also providing an experimental platform to study the function of chromatin structure in living cells. The creation of mouse models with artificial chromosomes in current study indicates that the genome structure in the nucleus possesses strong plasticity to tolerate alterations at the chromosome level such as Rb fusions, suggesting a model of genomic organization homeostasis in the mammalian nucleus. Genomic organization homeostasis explains the steady state of chromosome territory and spatial organization even with dramatic chromosome structural alterations. It also reflects the homeostatic flexibility of chromosomes to sustain the ability of natural resistance to chromosome structural changes through spontaneously readjusting their structure and location in the nucleus. Genomic organization homeostasis, consistent with the concept of self-organization in the genome[15] reflects a steady and flexible chromosome relationship and may lay the foundation for karyotype evolution. An intriguing task is to generate haploid cell and mouse libraries with the same genetic background that consist of different combinations of chromosome fusions, including mouse strains with all metacentric chromosomes. These resources can be used to comprehensively investigate the function of chromosome structures in cells and animals.

Xiaoyu Merlin Zhang[1,5], Meng Yan[2,5], Zhenhua Yang[3,5], Hao Xiang[1,5], Wei Tang[1], Xindong Cai[2], Qigui Wu[1], Xin Liu[4], Gang Pei[1] and Jinsong Li[1,2,3]✉

[1]*State Key Laboratory of Cell Biology, Shanghai Key Laboratory of Molecular Andrology, Shanghai Institute of Biochemistry and Cell Biology, CAS Center for Excellence in Molecular Cell Science, University of Chinese Academy of Sciences, Chinese Academy of Sciences, Shanghai, China.* [2]*School of Life Science, Hangzhou Institute for Advanced Study, University of Chinese Academy of Sciences, Hangzhou, Zhejiang, China.* [3]*School of Life Science and Technology, ShanghaiTech University, Shanghai, China.* [4]*State Key Laboratory of Molecular Biology, Shanghai Institute of Biochemistry and Cell Biology, CAS Center for Excellence in Molecular Cell Science, University of Chinese Academy of Sciences, Chinese Academy of Sciences, Shanghai, China.* [5]*These authors contributed equally: Xiaoyu Merlin Zhang, Meng Yan, Zhenhua Yang, Hao Xiang.*
✉*email: jsli@sibcb.ac.cn*

DATA AVAILABILITY

The raw data of WGS, RNA-seq, and Hi-C are available with accession number CRA004756.

REFERENCES

1. Gimenez, M. D. et al. *J. Hered.* **108**, 25–35 (2017).
2. Garagna, S., Page, J., Fernandez-Donoso, R., Zuccotti, M. & Searle, J. B. *Chromosoma* **123**, 529–544 (2014).
3. Garagna, S., Zuccotti, M., Capanna, E. & Redi, C. A. *Cytogenet. Genome Res.* **96**, 125–129 (2002).
4. Shao, Y. et al. *Nature* **560**, 331–335 (2018).
5. Luo, J., Sun, X., Cormack, B. P. & Boeke, J. D. *Nature* **560**, 392–396 (2018).
6. Kalitsis, P., Griffiths, B. & Choo, K. H. *Proc. Natl Acad. Sci. USA* **103**, 8786–8791 (2006).
7. Yang, H. et al. *Cell* **149**, 605–617 (2012).
8. Zhong, C. et al. *Cell Stem Cell* **17**, 221–232 (2015).
9. Hayashi, T. et al. *Genomics* **17**, 490–492 (1993).
10. Warburton, P. E. et al. *Curr. Biol.* **7**, 901–904 (1997).
11. Earnshaw, W. C., Ratrie, H. 3rd & Stetten, G. *Chromosoma* **98**, 1–12 (1989).
12. Rao, S. S. et al. *Cell* **159**, 1665–1680 (2014).
13. Quinodoz, S. A. et al. *Cell* **174**, 744–757.e24 (2018).
14. Chmatal, L. et al. *Curr. Biol.* **24**, 2295–2300 (2014).
15. Misteli, T. *Cell* **183**, 28–45 (2020).

ACKNOWLEDGEMENTS

We thank N. Li and D. Li for critical discussions. We thank L. Hui for providing the immortalized plasmid. We thank Genome Tagging Project (GTP) center for providing CENP-A-HAtag cell line. This study was supported by the National Key R&D Program of China and the National Natural Science Foundation of China (2019YFA0109900, 2020YFA0509000, 31821004, 32030029, and 31730062), and partly supported by China Postdoctoral Science Foundation (2021TQ0329).

AUTHOR CONTRIBUTIONS

J.L., X.M.Z., M.Y., and P.G. conceived of the project. X.M.Z., Z.Y., H.X., W.T., X.C., and Q.W. performed the experiments. M.Y., X.L. and X.M.Z. analyzed the high-throughput data. G.P. and X.L. interpreted the data with the help from all other authors. J.L., X.M.Z., and M.Y. wrote the manuscript. J.L. supervised the project.

COMPETING INTERESTS

The authors declare no competing interests.

ADDITIONAL INFORMATION

Supplementary information The online version contains supplementary material available at https://doi.org/10.1038/s41422-022-00722-x.

Correspondence and requests for materials should be addressed to Jinsong Li.

Reprints and permission information is available at http://www.nature.com/reprints